



## Research Paper

## CLEANING AND SPUTTERING USING PLANAR ACOUSTOPLASMA MAGNETRON

A.S. Abrahamyan<sup>\*</sup>, A.H. Mkrtychyan, V.V. Nalbandyan, H.T. Hovhannisyan,  
R.Yu. Chilingaryan, A.S. Hakobyan, P.H. Mossoyan

Institute of Applied Problems of Physics,  
25 Hrachya Nersissian Str., Yerevan, Republic of Armenia, 0014

---

**Abstract**

The paper describes the obtained experimental results for a planar acoustoplasma magnetron. The small radius of the anode loop allows focusing and accelerating the ionic component of the sprayed material.

Argon was used as a buffer gas. The characteristics of the magnetron in case of direct current supply and in acoustoplasma mode (AP) (with modulated current containing constant and variable components) are compared. The sputtering speed in AP mode increases. For the copper cathode, the gas pressure made  $< 1$  Pa and current density of the order of  $100 \text{ mA/cm}^2$  with increasing distance from the anode to the deposited substrate from 2 to 4 cm in case of DC supply, the deposition speed drops 3.3 times (from 17 to 5 nm/s), in the acoustoplasma mode – 2 times (from 13 to 6.4 nm/s).

For the anode-substrate distance 4 cm, the gain in the deposition speed in the AP mode, compared with DC is 1.2–1.5 times. The dependences of ion and electron currents on the substrate for different discharge parameters were measured. The study was based on a scheme with two potential grids with fixed and variable potentials. The possibility of forming an annular vapor-plasma flow of fast particles is shown.

*Key words:* magnetron discharge, acoustoplasma, sputtering technologies.

---

**1. Introduction**

The general concept of the influence of acoustic fields on physical media is as follows [1]: acoustic fields, due to long-range action and collective effects, lead to deformation of the characteristics of the medium. Therefore, a small amount of acoustic energy can lead to a significant change in the parameters of the medium and the parameters of radiation with an energy of quanta much greater than the energy of the acoustic quantum.

If such a medium is represented by plasma, then the propagation of the acoustic signal in the plasma leads to the interaction of plasma with acoustic field, i.e. to the acoustoplasma interaction. When modulating (in the region of acoustic frequencies) a discharge current containing a constant and a variable component, acoustic oscillations arise in the plasma. A discharge tube with a plasma also serves as an acoustic resonator. One of the manifestations of the acoustoplasma interaction is the formation of standing waves in the plasma in the form of superlattices of plasma parameters. Such superlattices can significantly change the parameters of the plasma medium, which made it possible to treat such a medium as a new one – acoustoplasma. Thus, a plasma with acoustic

---

\* Corresponding author. Institute of Applied Problems of Physics, 25 Hrachya Nersissian Str., Yerevan, Republic of Armenia, 0014. E-mail address: [arbel11@mail.ru](mailto:arbel11@mail.ru)

disturbance is called an acoustoplasma. In a glow discharge, the acoustoplasma mode leads to a low-frequency modulation of parameters of a positive column. In a magnetron discharge, the acoustoplasma mode leads to a modulation of parameters of the cathode region. The paper presents the experimentally obtained results for the developed cylindrical planar acoustoplasma magnetron [1, 2].

The authors tested various types of developed magnetrons: planar with cathode in the form of a circle and a cylindrical magnet, which were called ‘cylindrical planar’; planar with a rectangular cathode and a magnet; planar slotted ones; planar with a cathode in the form of a concave sphere of a large radius, as well as various types of cavity structures, among which were classical cylindrical ones. This paper is devoted to experiments with a planar cylindrical magnetron.

A comparison of the magnetron discharge with other types of discharges and their features for DC power supply are discussed in detail in [3–6].

However, there are no papers that compare all three types of discharge simultaneously from the same positions. In literature, cases of supplying a discharge with only a direct current, or when feeding with an alternating current of high frequency are considered. Thus, it is of some interest to supply the discharge in the magnetron with a low-frequency current ranging from 100 Hz. When feeding a discharge in a magnetron with a low-frequency current containing a constant and a variable component, an acoustoplasma mode appears [1, 2].

This paper compared the characteristics of the magnetron in case of direct current mode (DC) and acoustoplasma mode (AP) d. The AP mode of the magnetron is obtained by feeding the magnetron with a modulated current containing a constant and a sinusoidal alternate component.

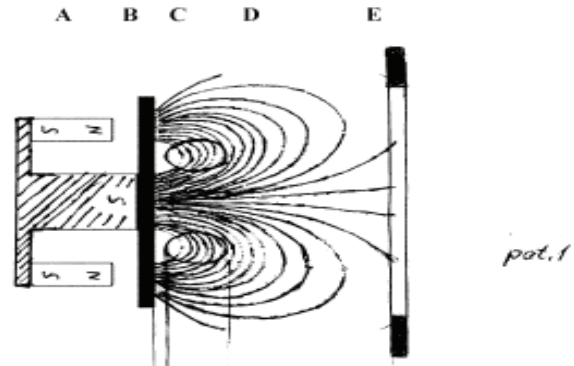
## 2. Experimental setup

Fig.1 shows a planar cylindrical magnetron [3]. A circular permanent ferrite-barium magnet was used. A cylindrical steel core was used instead of a central magnet. The circular magnet had the following dimensions:  $D_{out}=45\text{ mm}$ ,  $D_{in}=18\text{ mm}$ , ring height  $h=10\text{ mm}$ , magnetic induction  $\sim 0.3\text{--}0.5\text{ Tl}$ . Core diameter  $d=7\text{ mm}$ , height  $h=12\text{ mm}$ . The magnetic core (shaded area) closed the magnetic circuit. As a result, the plasma torus (Fig. 1) represented a ring with an outside diameter of  $26\text{ mm}$  and an inside diameter of  $12\text{ mm}$ .

The localization of a strong magnetic field, in our case at a distance of  $3\text{--}5\text{ mm}$  from the cathode, weakened so much that the discharge (when the cathode was displaced by this distance) became unstable. This indicated that the magnetic field strength was

becoming insufficient to retain electrons thus leading to pulsation of the spatial negative charge.

The anode represented a ring with a diameter of  $50\text{ mm}$  from a copper rod with a diameter of  $6\text{ mm}$ . The distance from the anode to the cathode could be varied from several  $\text{mm}$  to several  $\text{cm}$ .



**Fig. 1.** Scheme of magnetron discharge (pat.1). A – magnetic system; B – cathode; C – region of the ‘electron trap’ is the ‘torus’; D – ion generation region in the buffer gas; E – anode ring

Fig. 2 shows the diagram of the power supply of the developed magnetron. A power source including elements (1, 2, 3) is described in detail in [7]. When a modulating sinusoidal signal (6) is applied to the input of the pulse-width modulation (PWM) converter (2), the duration of the output pulses changes (at a constant clock rate of  $50\text{ kHz}$ ). This PWM modulated voltage is applied to the primary winding of the high-voltage transformer. A diode voltage multiplier is connected to the secondary winding of the transformer. The multiplier capacitors are selected in such a way that the output high voltage after the multiplier contains constant and variable components, but eliminates the  $50\text{ kHz}$  modulation frequency. The variable component repeats the frequency and the shape of the modulating signal. The value of the constant component is determined by the initial setting of the PWM modulator. High voltage, containing constant and variable components, is fed through the ballast resistance (4) to the magnetron (5).

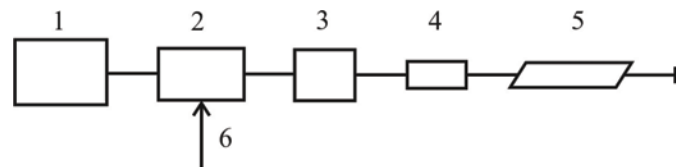


**Fig. 2.** Diagram of the experiment: 1 – power supply; 2 – pulse-width modulation voltage converter and power multiplier; 4 – resistive ballast; 5 – magnetron; 6 – modulating signal

## 3. Results and discussion

Fig. 3a shows the angular distribution given in [6, 8, 9] for ion energies: solid line –  $300\text{ eV}$ , dashed

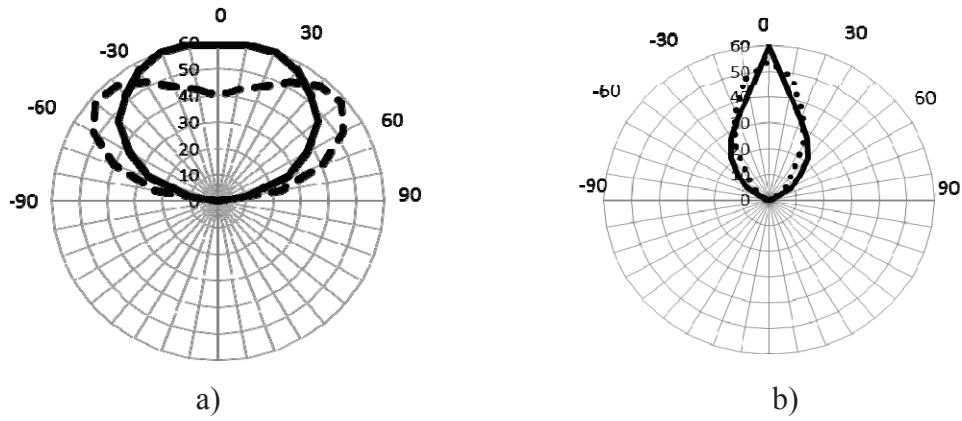


**Fig. 3.** The angular distribution of atoms formed during of cathode sputtering: a) at ion energies: solid line – 300 eV; dashed line – 100 eV [6]; b) for the manufactured magnetron: solid line – acoustoplasma mode (AP), 4 cm; dashed line – DC, 4 cm

line – 100 eV. Fig. 3b shows the angular distribution (central lobe) for the ion energies of the manufactured magnetron. Solid line – AP mode, direct current component density  $j_0=120 \text{ mA/cm}^2$ , density of variable current component  $j\sim 60 \text{ mA/cm}^2$ , current modulation frequency  $f=1.2 \text{ kHz}$ , anode – substrate distance 4 cm. Dashed line – DC mode, current density  $j=120 \text{ mA/cm}^2$

The power of the discharge in both cases is  $\sim 80 \text{ W}$ . The sputtering coefficient depends on the type of the incident ion and the cathode material [10, 11]. The cathode is made from copper. The gas pressure is  $\sim 0.5 \text{ Pa}$  (argon). The voltage in the near-cathode region is  $\sim 300\text{--}400 \text{ V}$ , i.e. the energy of ions  $> 300 \text{ eV}$ . In Fig. 3, the thickness of the deposited layer is plotted along the radius and angular degrees.

Fig. 3a shows that the 300 eV energy corresponds to the angular distribution and has the angle of  $\sim 100^\circ$  at half-height. Fig. 3b illustrates that the angular distribution is significantly narrowed ( $\sim 40^\circ$  at 0.5 level in the acoustoplasma mode and  $50^\circ$  at the DC discharge) in the manufactured magnetron due to the focusing action of the anode with a small radius (50 mm). A small diameter anode loop plays the role of an electrostatic lens and its focusing effect leads to aberrations of the cathode image. For the anode-substrate distance 4 cm, the gain in the deposition rate in the AP mode compared with DC at a current density of  $80 \text{ mA/cm}^2$  makes 1.5 times (4 nm/s vs. 2.6 nm/s).

Additional acceleration of positive ions in the anode potential field and inhibition of electrons occurs in the anode region. This leads to equalization of the electron and ion velocities not only by thermalization, while the characteristics of the manufactured magnetron can differ from those given in literature.

The current-voltage characteristics of the magnetron discharges are given in Fig. 4. The pressure of the buffer gas Ar is 0.5 Pa. The curve  $U$  corresponds

to the current-voltage characteristic taken from [6]. The curve  $U(\text{DC})$  corresponds to the current-voltage characteristic for a DC current for the manufactured magnetron.

The X-axis represents the discharge current in amperes (for the case of the AP mode, the constant component of the discharge current), along the Y-axis, the voltage applied to the cathode-anode gap in volts. For the AP mode, the modulation frequency is  $f=1.2 \text{ kHz}$ , the depth modulation  $M=0.25$  ( $M=I_0/I$  where  $I_0$  is the discharge current component, and  $I$  is the amplitude of the variable current component).

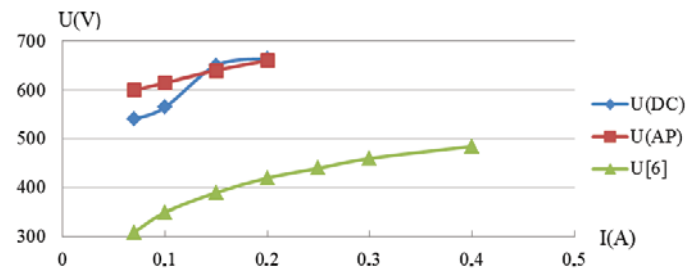


**Fig. 4.** Current-voltage characteristics of magnetron discharges. Buffer pressure – 0.5 Pa,  $U(\text{DC})$  – for the manufactured magnetron at direct current,  $U(\text{AP})$  – for the manufactured magnetron in acoustoplasma mode,  $U[6]$  – current-voltage characteristic from [6]

The voltage for the manufactured magnetron is higher than for the one described in [6] for the AP mode, which is higher than in DC.

It is found that even at a distance of 12 cm the ion concentration is still high enough and is almost comparable to the concentration of neutral atoms.

Usually X-ray reflectometry, X-ray diffractometry and atomic force microscopy are used to determine the thickness of thin sprayed layers [6, 12, 13]. In our experiments, the interference method of visible optical radiation in thin films was used. A method of coloring the surface of copper in various colors is known [14]. As a result of dosed oxidation of the sur-

face layer of copper, different colors are obtained. In our experiments, a small amount of oxygen was mixed with the buffer gas – argon, as a result, a layer of copper oxide was deposited on the surface of the substrate, which, depending on the thickness of the sputtering, had a different color. The aluminum foil of 0.4 mm thick was used as a substrate to study the speed and thickness of the sputtering. When deposited on such a foil, visible light is reflected from the aluminum surface and again passes through the sprayed layer. As a result, the thickness of the sputtered film gives a clear color picture – from blue (at an optical film thickness  $\sim 200$  nm) to red (at an optical thickness of  $\sim 350$ – $400$  nm). This method of estimation is approximate (accuracy  $\sim 10$ – $15$  %), but it is simple and convenient for express analysis, since it does not require complicated equipment.

A convenient experimental characteristic is proposed for approximate evaluation of magnetrons for deposition – the exposure coefficient ( $\eta$ ) with the given value [thickness $\times$ (discharge power density $\times$ time) $^{-1}$ ]. The value [ $L^3J^{-1}$ ] is obtained, where  $L$  – length,  $J$  – energy, i.e. inverse of energy density. However, for the application it is more convenient to use [ $nm \times \{(W/cm^2) \times s\}^{-1}$ ]. Thus, to determine the thickness of the sprayed layer (in nm), the coefficient  $\eta$  shall be multiplied by the power density of the cathode ( $W/cm^2$ ) and by the spraying time (in seconds). For the produced magnetron, the exposure coefficient was experimentally obtained for the following case: buffer gas pressure of 0.5 Pa, copper cathode  $\eta(Cu)=0.12(nm \times cm^2)/(W \times s)$ , distance cathode substrate  $d=2$  cm and  $d=4$  cm  $\eta(Cu)=0.04(nm \times cm^2)/(W \times s)$ . The thickness of the sprayed layer was determined from the center of the image. For example, with a cathode-substrate distance of 2 cm, a sputtering time of 50 s, a buffer gas pressure of 0.5 Pa, and a discharge current of 140 mA, we obtain the thickness of the sprayed layer  $\{0.12(nm \times cm^2)/(W \times s)\} \{75 W/cm^2\} \{50s\}=450$  nm. Using the current-voltage characteristics (Fig. 4), we determine that the current of 140 mA corresponds to the voltage of 640 V, the area of the cathode ring of erosion is 1.2 cm<sup>2</sup> and the power density is 75 W/cm<sup>2</sup>. The test showed good agreement between the estimates when using  $\eta$  with experiment.

In Fig. 5, for convenience of comparison with works of other authors, instead of the coefficient  $\eta$ , the rate of deposition of the film (rate of sputtering) is directly shown. The maximum sputtering rates obtained for silver clusters make 74 nm/s [15, 16] and for zinc clusters – 100 nm/s [17], for clusters of copper they are 2 times lower than for silver [12]. And these results were obtained for magnetrons with a power of several kW. In our case, the power of the magnetron is of the order of hundreds of watts. In

this case, according to [12], the deposition rate is  $\sim 1$ – $5$  nm/s. Much better results were obtained for the manufactured magnetron.

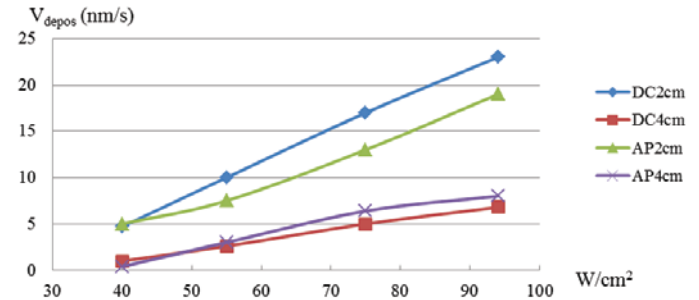


Fig. 5. Dependence of the deposition rate in nm/s ( $V_{depos}$ ) on power density with cathode and cathode-substrate distance for DC and AP modes

It is seen from Fig. 5 that with a power density of a 95 W/cm<sup>2</sup> cathode, when the distance to the substrate is changed from 2 to 4 cm in the DC mode, the sputtering speed is reduced by 3.4 times, and in the AP mode – by 2.3 times. With a power density of 75 W/cm<sup>2</sup> it decreases 3.3 and 2 times respectively. With a power density of 55 W/cm<sup>2</sup>, it decreases 3.8 and 2.5 times respectively and with a power density of 40 W/cm<sup>2</sup> it is reduced 4.7 and 12.5 times respectively. Thus, since the distance increases and the power density (discharge current) decreases, the AP mode becomes more and more advantageous.

In the processes of sputtering and doping and the settings of these processes, ion current control is necessary. In our experiments, the ion current on the substrate  $I_i$ , the electron current  $I_e$ , and the deposition rate  $V_{depos}$  (nm/s) were measured.

Typically, devices for measuring the ion current strength are constructed as follows [12], Fig. 6a. The ion current strength is recorded with the help of the Faraday-cylinder collectors, which prevents the escape of secondary electrons from the collector material. A locking electrode is placed in front of the Faraday cylinder under a negative potentiometer, which wraps the secondary electrons back to the collector.

When using the AP mode, the discharge power is modulated not only by the anode-cathode voltage, but also by the anode-diaphragm (2) (Fig. 6). This can lead to a significant distortion in current measurements. Therefore, the measurement scheme when using the AP mode was changed. In addition, the magnetron operated in the deposition mode, without selection of the ion flux, and therefore ions and electrons and neutral atoms could enter the collector. The current measurement scheme used in experiments with an acoustoplasma magnetron is shown in Fig. 6.

With the anode A relative to the cathode K, a voltage was supplied from the power supply source of the discharge, containing a constant and a variable

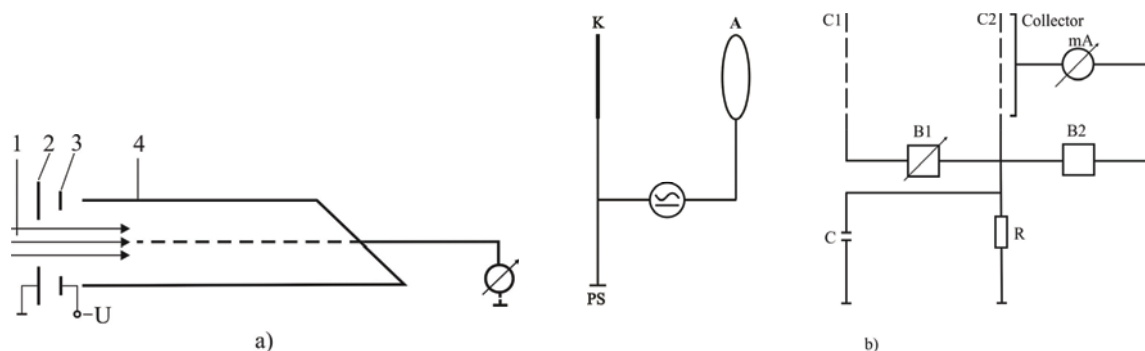


**Fig. 6.** a) Diagram of the device for measuring the ion current strength [12]: 1 – ion beam, 2 – diaphragm, 3 – locking electrode, 4 – Faraday cylinder; b) Scheme for measuring the strength of ion and electron currents in experiments with acoustoplasma magnetron: K – sputtered cathode, A – anode, C1 – the first grid, C2 – the second grid, mA – milliammeter, B1 – battery 1, B2 – battery 2, PS – power supply of discharge, R, C – resistance and leakage capacitor

component. The modes of operation of the magnetron and the RC chain of leakage resistance were chosen so that during the measurement period the potential of the grid C1 remained constant, i.e. did not change due to ions and electrons settling on a grid. Between the grids C1 and C2 a delaying or accelerating potential was created through the power supply B1. The potential that retards ions accelerates the electrons and vice versa. Battery B2 created a blocking potential preventing the current of secondary electrons. For this purpose, the voltage of B2 was of the order of 1.5–3 V. The voltage of the battery B1 could change thus changing the retarding potential to estimate the velocity distribution of particles. The milliammeter, installed on the collector, measured the difference in the components of ion and electron currents. Tungsten meshes with a cell of 300  $\mu\text{m}$  and a width of 50  $\mu\text{m}$  were used. The loss of particles on both meshes together amounted to about 40 %.

Such a circuit is more complicated both in manufacturing and in use, as compared to Fig. 6a, but it allows practically eliminating the influence of voltage variation on the anode and allows measuring not only the ion current, but also the electron current, as well as obtaining experimental ion distributions and electrons in energy and magnitude of the flux of neutral particles.

In experiments, the anode-cathode distance  $d(\text{a-cat})=1\text{ cm}$ , the anode-grid distance varied  $d(\text{a-C1})$  from 1 to 10 1–10 cm, the distance grid 1 – grid 2  $d(\text{C1-C2})=2\text{ cm}$ , the distance grid 2 – collector surface, which was the substrate for sputtering  $d(\text{C2-col})=0.3\text{ cm}$ . The diameter of the inlet aperture is C1 – 3 cm, the inlet diameter of the Faraday cylinder and the diameter of the substrate for the deposition is 0.8–1 cm.

The grid 2 is connected to the middle point of the batteries B1 and B2. Thus, if the potential (–) is on the grid 1, then the potential (+) is on the grid 2 and

the ions in the field between the grids 1 and 2 are decelerated while the electrons are accelerated. If the potential (+) is on the grid 1, then on the grid 2 the potential (–) is decelerated by the electrons and the ions are accelerated.

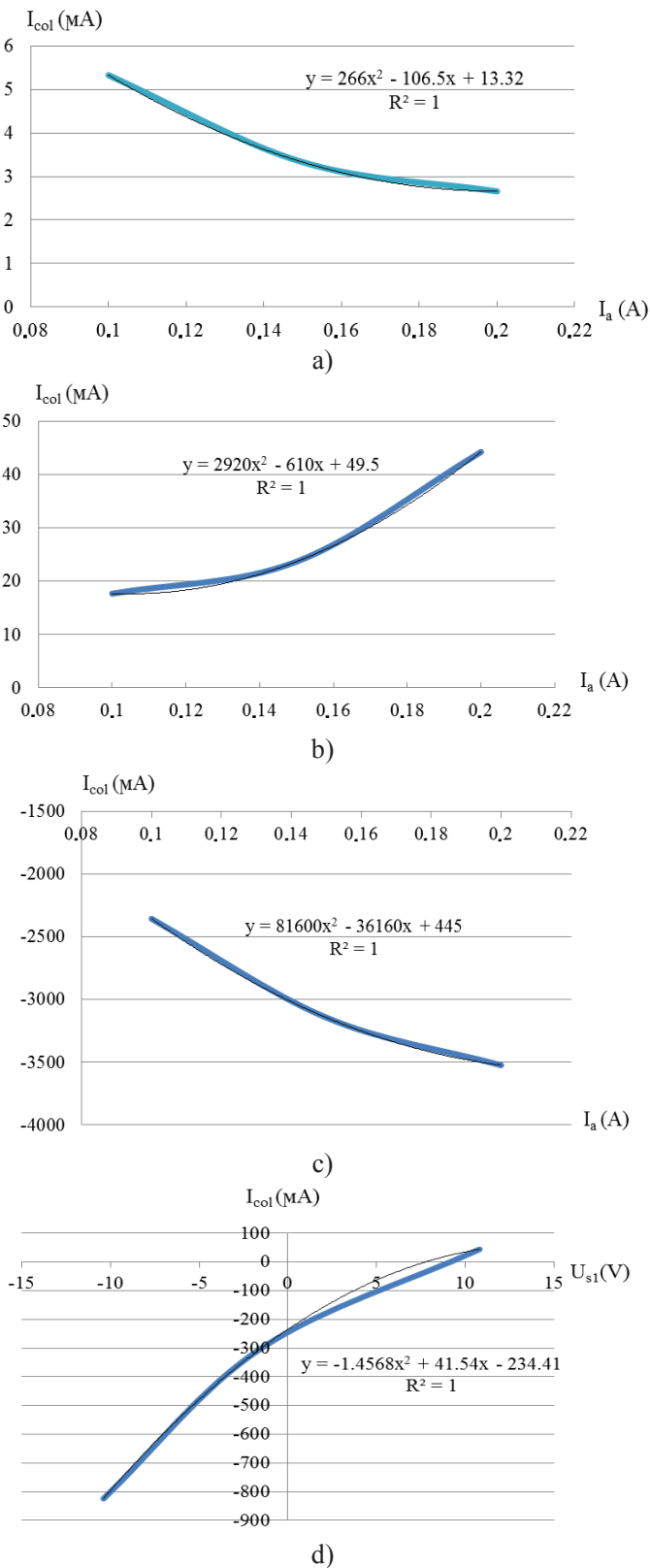
Fig. 7 shows the results of measurements of ion and electron currents on the collector. The abscissa represents the discharge current (anode current) in amperes, and the ordinate is the collector current in mA.

Fig. 7a shows that the voltage on the grid 1 is positive (relative to the collector). As a result, in the interval between grids 1 and 2, the ions are accelerated, and the electrons are delayed. The negative voltage on the grid 2 means that the secondary electrons knocked out from the collector surface are retained in the gap between the grid 2 and the collector surface. In Fig. 7b the voltage on the grid 1 is positive, similar to the voltage on the grid 2, as a result, the electrons knocked out of the collector do not return to the collector, but fall onto the grid 2.

From the comparison of Figs. 7a and 7b it can be seen that with the decrease of the discharge current, the electronic component of the particle flow to the substrate increases, and the ion component decreases.

Fig. 7c shows that with a negative voltage on the grid 1, the electrons in the interval grid 1-grid 2 are accelerated, and the ions are delayed, as a result, regardless of the potential on the grid 2, a large electronic current and a potential of –10 V on the grid 1 is sufficient to hold ions; ions have an average energy of < 10 eV.

Fig. 7d corresponds to the AP-mode of the discharge. The modulation frequency  $f=1.25\text{ kHz}$ , the modulation depth  $M=0.25$ , the discharge current constant component  $I_0=0.15\text{ A}$ , the grid potential  $2U_{s2}=-1.5\text{ V}$ , which means that it delays the secondary electrons. The voltage on the grid 1  $U_{s1}$  varies from (–) 10.4 V to (+) 10.8 V.



**Fig. 7.** Ion and electronic currents to the collector: a)  $d=2$  cm,  $U_{s1}=10.8$  V,  $U_{s2}=-1.5$  V,  $P_0=0.5$  Pa; b)  $d=2$  cm,  $U_{s1}=10.8$  V,  $U_{s2}=1.5$  V; c)  $d=2$  cm,  $U_{s1}=-10$  V,  $U_{s2}=-1.5$  V; d) AP,  $f=1.25$  kHz,  $M=0.25$ ,  $I_0=0.15$  A,  $U_{s1}=-1.5$  V,  $U_{s1}=-10.4/+10.8$  V

From Fig. 7d it is seen that for a negative potential on the grid 1 in the AP mode, as well as for the case of DC, a considerable electronic current enters the collector. If the potential on the grid 1 is positive, most of the electrons (with energy  $< 7$  eV) are retained and the collector current becomes ionic.

#### 4. Conclusions

- A cylindrical planar acoustoplasma magnetron was developed.
- A small radius of the anode loop allows focusing and accelerating the ionic component of the sprayed material. The possibilities of focusing and its aberration are shown.
- The characteristics of the magnetron are compared when the discharge is supplied in the direct current mode (DC) and in acoustoplasma mode (AP) (with a modulated current supply containing constant and variable components).
- The radiation pattern of the particle flow from the sputtered cathode is significantly narrowed (angle at the level of 0.5 from the maximum in the directivity pattern in existing magnetrons is  $\sim 100^\circ$ , and in the developed magnetron  $\sim 50^\circ$  in the DC mode and  $\sim 40^\circ$  in the AP mode).
- The current-voltage characteristic for the AP mode is increasing at a buffer gas pressure of 0.5 Pa and decreasing at a buffer gas pressure of 10 Pa. This characteristic for the DC mode is increasing at 0.5 Pa and parallel to the current axis at a pressure of 10 Pa, i.e. when the discharge current changes, the voltage remains constant.
- At a cathode power density of  $95$  W/cm<sup>2</sup>, when the distance to the substrate is changed from 2 to 4 cm in the DC mode, the sputtering speed decreases by a factor of 3.4, and in the AP mode by a factor of 2.3. With a power density of  $75$  W/cm<sup>2</sup>, it decreases 3.3 and 2 times respectively. With a power density of  $55$  W/cm<sup>2</sup> – 3.8 and 2.5 times respectively. With a power density of  $40$  W/cm<sup>2</sup> – 4.7 and 12.5 times respectively. Thus, as the distance increases and the power density decreases (i.e. the discharge current), the AP mode becomes more and more advantageous.
- A new scheme for measuring the strength of ion and electron currents in experiments with an acoustoplasma magnetron taking into account the specificity of the acoustoplasma discharge is proposed.
- Diagrams of ion and electron currents on the substrate are shown.

## References

- [1] Mkrtchyan A.H., Mkrtchyan A.R., Abrahamyan A.S., Nalbandyan V.V. Patent Armenia, no. 3086A, 2016.
- [2] Mkrtchyan A.R., Abrahamyan A.S. Creation of new generation magnetrons based on acoustoplasmic states for surface cleaning and deposition on substrates. *The First Russian Crystallographic Congress, Moscow*, 2016, p. 177. In Russian.
- [3] Danilin B.S., Syrchin V.K. *Magnetron spray systems*. Moscow, Radio and communication, 1982, 72 p.
- [4] Chapman B. *Glow discharge processes: sputtering and plasma etching*. New York, Wiley, 1980, 432 p.
- [5] Raizer Yu.P. *Physics of gas discharge*. Moscow, Nauka, 1987, 537 p. In Russian.
- [6] Kashtanov V.P., Smirnov B.M., Hippler R. Magnetron plasma and nanotechnology. *Physics-Uspekhi*, 2007, vol. 50, no. 5, pp. 455–488. doi: 10.1070/PU2007v050n05ABEH006138.
- [7] Abrahamyan A.S., Hakobyan K.V., Hovhannisyan H.T. The power supply for a CO<sub>2</sub> laser with an acousto plasma discharge model. *Bulletin of the State Engineering University of Armenia. Series «Modeling, optimization, management»*, 2011, vol. 1, no. 14, pp. 18–24. In Armenian.
- [8] Ekpe S.D., Dew S.K. Theoretical and experimental determination of the energy flux during magnetron sputter deposition onto an unbiased substrate. *Journal of Vacuum Science & Technology A*, 2003, vol. 21, no. 2, pp. 476–483, doi: 10.1116/1.1554971.
- [9] Stepanova M., Dew S.K. Estimates of differential sputtering yields for deposition applications. *Journal of Vacuum Science & Technology A*, 2001, vol. 19, no. 6, pp. 2805–2816, doi: 10.1116/1.1405515.
- [10] Westwood W.D. Glow discharge sputtering. *Progress in Surface Science*, 1976, vol. 7, no. 2, pp. 71–111. doi: 10.1016/0079-6816(76)90002-2.
- [11] Feldman L.C., Mayer J.W. *Fundamentals of surface and thin film analysis*. New York, Nort-Holland, 1986, 352 p., doi: 10.1002/crat.2170220503.
- [12] Popov V.F., Gorin Yu.N. *Processes and installations of electron-ion technology: Textbook for high schools*. Moscow, High school, 1988, 255 p. In Russian.
- [13] Shyjumon I. Ph.D., Thesis. Grejfwald Univ., Grejfwald, 2005.
- [14] Jan Skerik. *Receptar pro elektrotechnika*. Praha, SNTL, 1974, 448 p.
- [15] Hagen O.F. Formation of silver clusters in nozzle expansions. *Zeitschrift für Physik D Atoms, Molecules and Clusters*, 1991, vol. 20, no. 1, pp. 425–428. doi: 10.1007/BF01544028.
- [16] Hagen O.F. Cluster ion sources (invited). *Review of Scientific Instruments*, 1992, vol. 63, no. 4, pp. 2374–2379. doi: 10.1063/1.1142933.
- [17] Gspann J. High-intensity ionized cluster beams for surface modification: deposition and erosion. *Nuclear Inst. and Methods in Physics Research, B*, 1993, vol. 80–81, no. PART 2, pp. 1336–1339. doi: 10.1016/0168-583X(93)90795-8.

Received 12.04.2018